Plasma Chem Plasma Process (2015) 35:365–386
DOI 10.1007/s11090-014-9605-6

REVIEW PAPER

Interaction of a H_2O/Ar Plasma Jet with Nitrogen Atmosphere: Effect of the Method for Calculating Thermophysical Properties of the Gas Mixture on the Flow Field

N. Agon · J. Vierendeels · M. Hrabovský · A. B. Murphy · G. Van Oost

Received: 6 December 2013 / Accepted: 23 December 2014 / Published online: 8 January 2015

Abstract The effect of calculating thermodynamic and transport properties of a gas mixture with mixing rules on the flow field in the modeling of a thermal plasma jet was studied. A 3D large eddy simulation model of a non-transferred direct current hybrid water/argon plasma torch issuing in nitrogen atmosphere at 400 K was developed to compare three different models for the calculation of transport and thermodynamic properties of the ternary gas mixture. In the first model, thermodynamic and transport properties of the pure gases are used with mixing rules to estimate the mixture properties. In the second model, the properties of plasma gas (Ar/H_2O) are calculated rigorously and mixing rules are used for estimating the properties of the mixture of plasma gas and nitrogen. In the third model, the thermodynamic and transport properties of the ternary gas mixture are calculated rigorously without any mixing rules. From numerical results, the error introduced by using mixing rules was evaluated through comparison of calculated temperature, velocity and concentration profiles of the flow field at different positions downstream of the torch exit nozzle. It was found that the differences in transport properties between the exact solutions and the results from calculation with mixing rules can yield significantly different flow fields.

Keywords Thermal plasma · Computational fluid dynamics · Thermophysical properties · Mixing rules · Ionized gas mixtures

N. Agon (✉) · G. Van Oost
Department of Applied Physics, Ghent University, Sint-Pietersnieuwstraat 41, Ghent, Belgium
e-mail: Nicholas.Agon@Ugent.be

J. Vierendeels
Department of Flow, Heat and Combustion Mechanics, Ghent University, Sint-Pietersnieuwstraat 41, Ghent, Belgium

M. Hrabovský
Institute of Plasma Physics ASCR, Za Slovankou 1782/3, Prague, Czech Republic

A. B. Murphy
CSIRO Manufacturing Flagship, P.O. Box 218, Lindfield, NSW 2070, Australia

Introduction

Thermal plasmas provide opportunities for materials processing due to their high energy content and high energy density. Plasma processing techniques of current interest include spraying, coating, synthesis, sintering, extractive metallurgy and waste treatment. Plasma flow is highly complex and a large amount of computational fluid dynamics (CFD) modeling has already been done to examine the effect of different operating conditions and to gain a better understanding of the physical phenomena [1, 2]. The overall goal of these numerical studies is to develop models that can correctly predict the plasma flow characteristics (temperature, velocity and concentration fields) and consequently the interaction with solid or liquid materials in plasma processes (e.g. plasma gasification).

In all plasma jet simulations described in literature over the last two decades, independent of the specific case setup, the same physical mechanisms and model aspects are included. The approach and assumptions used in their implementation strongly influences the accuracy of the simulation results. The effect on the flow field of the description of each of these physical phenomena (e.g. diffusion [3], turbulence [4, 5], etc.) and modeling aspects (e.g. geometry [6], dimensions of the domain, time-dependency [2], CFD code [1], equilibrium conditions, etc.) has therefore been individually studied. A full description of the main elements involved in the modeling of DC arc plasma torches can be found in the review by Trelles et al. [7].

The medium in thermal plasma problems rarely consists of a single gas, but is mostly made up of a mixture of gases. Therefore another important aspect in the fluid dynamic modeling of plasma jets is the definition of the gas mixture and the calculation of its thermodynamic and transport properties.

Murphy [8] stated that accurate values of the transport coefficients and the thermodynamic properties of high-temperature gases and gas mixtures are indispensable inputs in the CFD modeling of thermal plasma processes. Also Trelles [7] pointed out that the accuracy of results strongly depends on the use of suitable thermodynamic and transport properties. The influence of using mixing rules on the mixture properties has been published by Gleizes et al. [9], who identified large variations in properties of gas mixtures with metallic vapors depending on the chosen mixing rules. The effect of the method for calculating thermodynamic and transport properties of a gas mixture on the simulated flow field of a plasma jet, however, has not yet been the subject of a quantitative study.

The first step in the calculation of thermodynamic and transport properties is obtaining the equilibrium composition of the gas or gas mixture, which is usually done using the Gibbs free energy minimization approach. Once the species composition is known, the thermodynamic properties [enthalpy (H), density (ρ), molecular weight (M), speed of sound (c) and specific heat capacity (C_p)] of a closed gaseous system in thermodynamic equilibrium at constant pressure and temperature can be directly calculated from particle number densities and internal partition functions [10, 11]. The transport properties (thermal conductivity (k), viscosity (μ), etc.) are generally calculated using the well-known Chapman–Enskog method, which is an approximate solution of the Boltzmann equation [12].

In the modeling of plasma processes, the plasma gas from the torch is represented by either a pure gas, such as argon [13–17] or a gas mixture with fixed composition (e.g. 50%Ar–50%H_2) [2, 4, 18–23]. Thermodynamic and transport properties under Local Thermodynamic Equilibrium (LTE) assumptions are available for most of these plasma gases (either pure gases or gas mixtures with fixed composition) as a function of temperature and pressure [24].

In many applications, this plasma gas is mixed with other gases. For these multi-component mixtures, the local gas composition cannot be known a priori and therefore it is necessary to solve the species conservation equation(s) in the CFD simulations. The properties of the gas mixture are then determined from the local species concentrations, temperature and pressure. There are two general methods of doing this.

The rigorous method is to take the complete system of all gases considered and calculate a multidimensional matrix of mixture properties as a function of gas concentrations and temperature. This way, not only the products of ionization and dissociation of the pure gases, but also combined ions and molecules from the interactions between different gases are considered. The accurate thermodynamic and transport properties are then directly assigned to the gas mixture through interpolation of this pre-calculated matrix. Because all possible species, formed from the different gases are included in the calculation of the species composition of the complete system, this method will be referred to as the full multi-component approach. This approach was applied by Vincent et al. [23], Trelles et al. [25] and Colombo et al. [26] in their plasma flow simulations.

In simulations where the plasma interacts with a lot of different gases, the rigorous calculation of thermodynamic and transport properties of the gas mixture can become overly cumbersome. Also, the large dataset needed to calculate the properties according to the full multi-component approach is not always readily available. For example, in a CFD simulation of a plasma gasification reactor, it is not feasible to incorporate a full multi-component approach for the calculation of the thermodynamic and transport properties of the gas mixture, due to the complexity of the calculation routines and the computational expense. In such cases, the temperature-dependent properties of the pure gases are used with mixing rules to estimate the gas mixture properties. These rules are based on simple species proportionality in terms of mass fractions or molar fractions. Dynamic viscosity and thermal conductivity are often calculated with the formulas of Wilke [27] and Mason and Saxena [28]. These formulas and their limited accuracy have already been discussed and compared with more precise mixing rules in the literature [9, 29, 30]. Nevertheless, they continue to be used very frequently in plasma jet simulations because of their simplicity [1, 4, 18, 21].

It is therefore relevant to evaluate the accuracy of the results from simulations with thermodynamic and transport properties estimated with mixing rules compared to the results from simulations with the full multi-component approach. In the present paper, CFD simulations of a thermal plasma jet generated by a hybrid water/gas DC arc plasma torch (described in detail by Hrabovský et al. [31]) were performed. This hybrid water/gas stabilization offers the possibility of creating a low-density, high-velocity plasma with substantially different properties from conventional torches. It is being successfully used for plasma spraying and in the plasma treatment of waste. The development of this plasma model and the comparison between a full multi-component approach and methods in which mixing rules are used for the mixture properties calculation presented here are part of an effort aimed towards modeling a plasma gasification system.

Modeling Approach

The interaction of the H_2O/Ar plasma jet with ambient nitrogen at atmospheric pressure was simulated. Three different mixing models were calculated with the same case setup and compared on the basis of the resulting flow field. In the following sections, the details of the case setup are explained, i.e. the computational domain and boundary conditions, the different mixing models, boundary conditions and model assumptions and model equations.

Computational Domain and Boundary Conditions

The domain considered in the calculations represents the plasma jet region outside the plasma torch. The 3D geometry shown in Fig. 1 is cylindrical with a diameter of 10 cm and a length of 20 cm. These dimensions correspond well with the area of interest for plasma spraying and for interaction of plasma with biomass and/or waste in plasma gasification. The exit nozzle of the plasma torch is located at the top of the domain with a radius of 3 mm.

The grid consists of 453,375 hexahedral cells and is more refined near the central axis and closer to the torch nozzle. This grid size was proven to be sufficiently fine using a grid independence study between 135,000 (coarse), 453,375 (fine) and 1,881,000 (finest) cells. An extract of this study is shown in Fig. 2, in which the time-averaged temperature profiles (over 7.5×10^{-4} s) at the position 5 mm downstream of the nozzle exit for the three different grid sizes were compared. The time step size was adapted so the Courant–Friedrichs–Lewy (CFL) number remained the same for the three grid sizes. Although there is still a small difference between the fine grid and the finest grid, the fine grid with 453,375 cells was selected because of computational time considerations.

The flow of plasma from the nozzle exit was defined by means of temperature, velocity and concentration profiles. The species distribution over the nozzle radius was expressed in terms of a mass fraction profile of argon and steam. This profile was derived from experimental results published by Hrabovský et al. [31] and approximated by a fourth order polynomial function (Fig. 3c). The profiles of temperature (Fig. 3a) and velocity (Fig. 3b) were expressed with the following functions [1, 5, 32, 33]:

$$\text{Temperature profile}: \quad T_{in} = (T_0 - T_w)\left[1 - \left(\frac{r}{R_{in}}\right)^{n_T}\right] + T_w \tag{1}$$

$$\text{Velocity profile}: \quad v = v_0\left[1 - \left(\frac{r}{R_{in}}\right)^{n_v}\right] \tag{2}$$

where $T_w = 1{,}300$ K is the torch wall temperature (i.e. the melting temperature of steel) and $R_{in} = 0.003$ m is the torch radius. The centerline velocity and temperature were chosen as $v_0 = 4{,}300$ m/s and $T_0 = 19{,}140$ K respectively, based on experimental

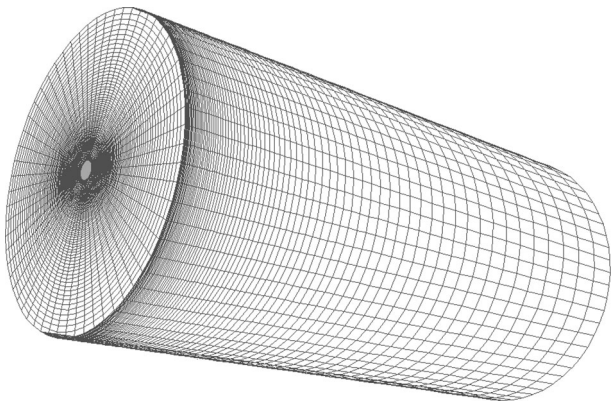

Fig. 1 Model geometry with hexahedral mesh

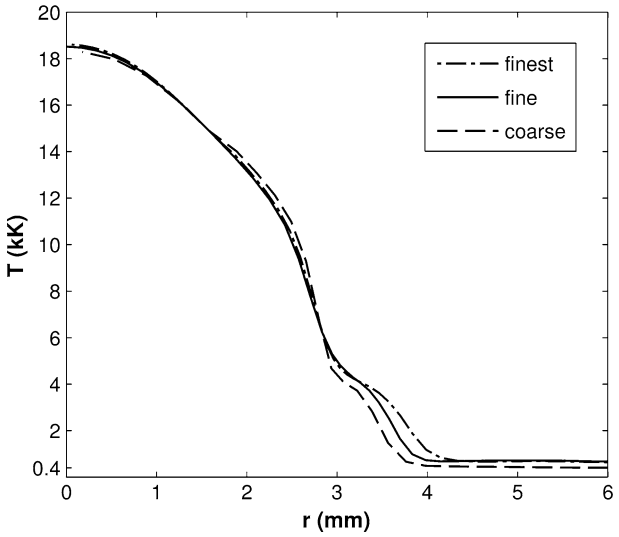

Fig. 2 Grid independence study

conditions [31]. The fitting parameters $n_T = 2.737$ and $n_v = 1.688$ were chosen so that the resulting enthalpy flux exiting the torch nozzle matches the power of the plasma torch with $I = 400$ A and argon flow rate of 22.5 standard liters per minute (slm). The experimental measurements that were used as a reference in these calculations were published by Hrabovský et al. [34].

Around the torch nozzle, a 2 mm wall boundary condition marks the outer framework of the plasma torch at a fixed temperature of 1,300 K. All the other borders of the computational domain were defined as pressure boundaries at atmospheric pressure with nitrogen at 400 K to simulate the surrounding atmosphere. As a simplification, nitrogen gas was chosen as the ambient gas to represent air. In that way, all chemical elements could be attributed to a single gas and an unambiguous comparison could be made between the different mixing models.

Description of the Mixing Models

Three different methods for calculating thermodynamic and transport properties of the gas mixture were compared to investigate the influence on the flow field of using mixing rules. The formulas for the mixture density and speed of sound were expressed in terms of molar fraction, for enthalpy in terms of mass fraction and for dynamic viscosity and thermal conductivity the respective mixing rules of Wilke [27] and of Mason and Saxena [28] were used. The specific heat was calculated as the numerical derivative of enthalpy over an interval of 0.2 K. The thermodynamic properties and transport coefficients of the different gases and gas mixtures were calculated using the methods presented by Murphy in previous publications [8, 29, 35, 36].

The mixing rules of Wilke and Mason and Saxena were derived for mixtures of non-ionized gases, considering only elastic collisions. They assume that the off-diagonal terms in the matrix that is inverted in calculating the respective transport properties is zero, and that all interactions between species belonging to different gases have the same

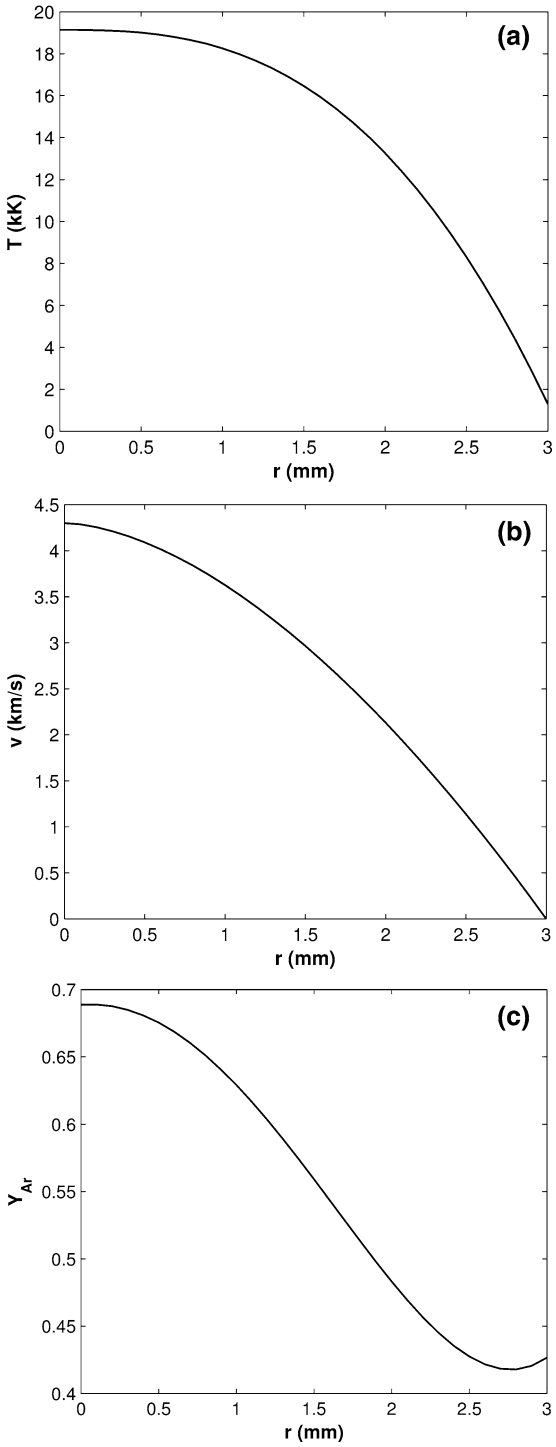

Fig. 3 Plasma inlet profiles **a** temperature, **b** velocity and **c** argon mass fraction

Table 1 Details of the three mixing models

Property	Model 1 i = Ar, H_2O and N_2	Model 2 i = 1: pla (Ar + H_2O) and i = 2: N_2	Model 3
Density (ρ)	$\rho_{mix} = \sum_i^n c_i \rho_i$ with $\rho_i = f(T)$	$\rho_{mix} = \sum_i^{n-1} c_i \rho_i$ with $\begin{matrix}\rho_1 = f(Y_{Ar}, T) \\ \rho_2 = f(T)\end{matrix}$	$\rho = f(Y_{Ar}, Y_{N_2}, T)$
Enthalpy (H)	$H_{mix} = \sum_i^n Y_i H_i$ with $H_i = f(T)$	$H_{mix} = \sum_i^{n-1} Y_i H_i$ with $\begin{matrix}H_1 = f(Y_{Ar}, T) \\ H_2 = f(T)\end{matrix}$	$H = f(Y_{Ar}, Y_{N_2}, T)$
Heat capacity (C_p)	$C_{p,mix} = \sum_i^n Y_i C_{p,i}$ with $C_{p,i} = \frac{dH_i}{dT}$	$C_{p,mix} = \sum_i^{n-1} Y_i C_{p,i}$ with $C_{p,i} = \frac{dH_i}{dT}$	$C_p = \frac{dH}{dT}$
Speed of sound (c)	$c_{mix}^2 = RT \frac{\sum_i^n c_i C_{p,i}}{\sum_i^n c_i M_i \sum_i^n c_i \left(C_{p,i} - R\right)}$ with $C_{p,i}, M_i = f(T)$	$c_{mix}^2 = RT \frac{\sum_i^{n-1} c_i C_{p,i}}{\sum_i^{n-1} c_i M_i \sum_i^{n-1} c_i \left(C_{p,i} - R\right)}$ with $\begin{matrix}C_{p,1}, M_1 = f(Y_{Ar}, T) \\ C_{p,2}, M_2 = f(T)\end{matrix}$	$c = f(Y_{Ar}, Y_{N_2}, T)$
Viscosity (μ)	$\mu_{mix} = \sum_{i=1}^n \frac{c_i \mu_i}{\sum_j c_j \phi_{ij}}$ with $\mu_i, M_i = f(T)$ with $\phi_{ij} = \frac{1}{\sqrt{8}} \left(1 + \frac{Mi}{M_j}\right)^{-\frac{1}{2}} \left[1 + \left(\frac{\mu_i}{\mu_j}\right)^{\frac{1}{2}} \left(\frac{M_j}{M_i}\right)^{\frac{1}{4}}\right]^2$	$\mu_{mix} = \sum_{i=1}^{n-1} \frac{c_i \mu_i}{\sum_j c_j \phi_{ij}}$ with $\begin{matrix}\mu_1, M_1 = f(Y_{Ar}, T) \\ \mu_2, M_2 = f(T)\end{matrix}$ with $\phi_{ij} = \frac{1}{\sqrt{8}} \left(1 + \frac{M_i}{M_j}\right)^{-\frac{1}{2}} \left[1 + \left(\frac{\mu_i}{\mu_j}\right)^{\frac{1}{2}} \left(\frac{M_j}{M_i}\right)^{\frac{1}{4}}\right]^2$	$\mu = f(Y_{Ar}, Y_{N_2}, T)$
Thermal conductivity (k)	$k_{mix} = \sum_{i=1}^n k_i \left[1 + \sum_{\substack{k=1 \\ k \neq i}}^{n} G_{ik} \frac{x_k}{x_i}\right]^{-1}$ with $k_i, \mu_i, M_i = f(T)$ with $G_{ik} = \frac{1.065}{2\sqrt{2}} \left(1 + \frac{M_i}{M_k}\right)^{-\frac{1}{2}} \left[1 + \left(\frac{\mu_i}{\mu_k} \frac{M_k}{M_i}\right)^{\frac{1}{2}} \left(\frac{M_i}{M_k}\right)^{\frac{1}{4}}\right]^2$	$k_{mix} = \sum_{i=1}^n k_i \left[1 + \sum_{\substack{k=1 \\ k \neq i}}^{n} G_{ik} \frac{x_k}{x_i}\right]^{-1}$ with $\begin{matrix}k_1, \mu_1, M_1 = f(Y_{Ar}, T) \\ k_2, \mu_2, M_2 = f(T)\end{matrix}$ with $G_{ik} = \frac{1.065}{2\sqrt{2}} \left(1 + \frac{M_i}{M_k}\right)^{-\frac{1}{2}} \left[1 + \left(\frac{\mu_i}{\mu_k} \frac{M_k}{M_i}\right)^{\frac{1}{2}} \left(\frac{M_i}{M_k}\right)^{\frac{1}{4}}\right]^2$	$k = f(Y_{Ar}, Y_{N_2}, T)$

cross-section [30]. They give reasonable results at lower temperatures, before dissociation and ionization occur, but are generally inaccurate at higher temperatures [9, 29, 30].

Pure gas data were tabulated as a function of temperature from 400 to 20,000 K with intervals of 100 K. Properties of the plasma gas (Ar/H_2O) and the complete gas mixture ($Ar/H_2O/N_2$) are also function of species mass fraction(s) and were stored in a multidimensional matrix with mass fraction step size(s) of 0.02. Except for enthalpy, for which 0.01 was used as the mass fraction step size. All properties were calculated at a pressure of 1 atm.

The specifics of the three different models are now explained and are summarized in Table 1 (where x and Y denote respectively mole fraction and mass fraction).

Model 1

The thermophysical properties of respectively Ar, H_2O and N_2 were calculated by considering only the interactions of species within each individual gas (which includes hydrogen–oxygen interactions for water vapour) [8, 29, 35, 36]. At every iteration of the model, the properties at each point were approximated as a function of temperature by linear interpolation. The mixture properties were then calculated by using mixing rules. Consequently, only the dissociation and ionization products (ions, atoms and molecules) of each individual gas are considered: e^-, Ar, Ar^+, Ar^{++}, Ar^{+++}, Ar^{++++}, $H_2O_{(g)}$, H_2, O_2, O, O^+, O^{++}, O^{+++}, O^-, O_2^+, O_2^-, O_3, O_3^+, O_3^-, H, H^+, H^-, H_2^+, H_2^-, H_3^+, OH, OH^+, OH^-, HO_2, HO_2^+, HO_2^-, H_2O^+, H_2O_2, $H_2O_2^+$, H_3O^+, N_2, N^+, N^{++}, N^{+++}, N_2^+, N_2^-, N_3, N_3^+, N_3^-.

Model 2

The mixing rules were only applied between two gases, nitrogen and 'plasma gas'. The properties of the plasma gas mixture of argon and steam were calculated rigorously (considering the argon–water vapour, argon–hydrogen, argon–oxygen and hydrogen–oxygen interactions) [8, 36]. At every iteration of the model, bilinear interpolation as a function of argon mass fraction and temperature from this pre-calculated table was performed. The same species as in model 1 were included in the property calculation, but the resulting properties of the Ar/H_2O mixture differ from the properties calculated using mixing rules because of additional interactions and consequently a change in Gibbs free energy of this binary system.

Model 3

In this full multi-component model, no mixing rules were used to calculate the thermodynamic and transport properties of the ternary mixture of argon, steam and nitrogen. Thermodynamic and transport properties were interpolated from a pre-calculated matrix as a function of argon mass fraction, nitrogen mass fraction and temperature. In the calculation of these properties all possible interactions (i.e. argon–water vapour, argon–hydrogen, argon–oxygen and hydrogen–oxygen, nitrogen–water vapour, nitrogen–oxygen and nitrogen–hydrogen) were taken into account [29, 36, 37]. This means that the combined products of H_2O and N_2 (NO, NO^+, NO^-, NO_2, NO_2^+, NO_2^-, N_2O, N_2O^+, N_2O^-, N_2O_3, N_2O_4, NO_3, NO_3^-, NH^+, NH, NH^-, NH_2, NH_3, NH_4^+, N_2H_2, N_2H_4, HN_3, HNO, HNO_2, HNO_3, NH_2OH, NH_2NO_2) were also included in the properties calculation together

with the list of species listed for model 1. Although the concentration of these additional components is low, it can change the resulting thermophysical properties of the gas mixture.

Model Assumptions and Equations

Ansys FLUENT was used as the CFD software, complemented with user-defined functions (UDF) for plasma inlet boundary conditions, thermodynamic and transport properties (including diffusion) and for post-processing purposes. Large eddy simulation (LES) was chosen as the turbulence model with Dynamic Smagorinsky-Lilly for the subgrid-scale model in combination with the pressure-based solver. The time-step size was 1.5×10^{-7} s, bounded central differencing was selected as the spatial discretization scheme and second order implicit scheme was selected for temporal discretization. The simulations presented in this study were based on the following main assumptions:

- Effects of gravity and the effect of viscous dissipation on the temperature were neglected.
- The system is assumed to be in LTE [38]. This assumption is generally accepted in the modeling of atmospheric plasma jets [2]. Effects from ionization, dissociation and chemical reactions of gas species are included in the calculation of the gas properties (see previous paragraph).
- No electromagnetic effects were taken into account.
- Compressibility effects were neglected.

For this 3D time-dependent flow, the governing equations can be represented by mass continuity equation, the conservation equation of momentum, species conservation equation and energy conservation equation:

Mass continuity equation:

$$\frac{\partial \rho}{\partial t} + \nabla \cdot (\rho \vec{v}) = 0 \tag{3}$$

where ρ is the local density of the gas mixture and $\vec{v}$ the gas velocity vector.

Momentum conservation equation:

$$\frac{\partial (\rho \vec{v})}{\partial t} + \nabla \cdot (\rho \vec{v}\vec{v}) = -\nabla p + \nabla \cdot \vec{\tau} \tag{4}$$

where p is the pressure and $\vec{\tau}$ is the stress tensor, calculated from components with respectively molecular and turbulent viscosity.

Species:

$$\frac{\partial (\rho Y_i)}{\partial t} + \nabla \cdot (\rho \vec{v} Y_i) = -\nabla \cdot \vec{J}_i \tag{5}$$

The diffusion flux of species i, $\vec{J}_i$, includes a laminar and a turbulent contribution to diffusion. The laminar diffusion was described by the combined diffusion approach of Murphy [39]. This method describes the diffusion of high-temperature gases relative to one another. Combined diffusion coefficients allow the diffusion of one gas (e.g., argon) with respect to another (e.g., nitrogen) to be defined. A gas is defined as comprising all species derived from that gas; e.g. nitrogen gas comprises N_2, N, N^+, N^{2+}, etc., and electrons derived from the nitrogen species. The combined diffusion coefficients have the advantage

that only one 'gas' conservation equation needs be solved, rather than N–1 species conservation equations for a plasma containing N species [29]. They are linear combinations of the multi-component diffusion coefficients. More details on the theory of the combined diffusion coefficient method can be found in publications by Murphy [39]. With some additional assumptions on this approach, the expression for the diffusion flux in a three-component mixture could be written in terms of binary combined diffusion coefficients (see Appendix 1). The diffusion flux of species i could then be defined as:

$$J_i = \sum_{j}^{n-1} \left(\frac{\rho}{\bar{M}^2} \bar{m}_i \bar{m}_j \bar{D}_{ij}^{x}(\bar{x}_j, T) \nabla \bar{x}_j - \bar{D}_{ij}^{T}(\bar{x}_j, T) \nabla \ln T \right) + \frac{\mu_t}{Sc_t} \nabla Y_i \tag{6}$$

The first term on the right-hand side describes the laminar diffusion by using the combined diffusion approach and was calculated with a user-defined function in FLUENT as a source term in the species conservation equation. $\bar{M}$ is the average mass of all species in the gas mixture, $\bar{m}_i$ and $\bar{m}_j$ are respectively the average masses of the heavy species of the gas i and j, $\bar{x}_j$ is the sum of the mole fractions of the species of gas j and $n = 3$ is the number of gases in the mixture. The combined ordinary diffusion coefficient $\bar{D}_{ij}^{x}$ and combined temperature diffusion coefficient $\bar{D}_{ij}^{T}$ (as functions of the molar fraction of gas j and temperature) describe, respectively, diffusion due to mole fraction gradients and temperature gradients.

The second term on the right-hand side was calculated by the standard FLUENT code and describes turbulent diffusion with Sc_t the turbulent Schmidt number and μ_t the turbulent viscosity.

Energy conservation equation:

$$\frac{\partial(\rho E)}{\partial t} + \nabla \cdot (\vec{v}(\rho E + p)) = \nabla \cdot \left(k_{eff} \nabla T - \sum_i h_i \vec{J}_i \right) - R \tag{7}$$

where k_{eff} is the effective conductivity ($k + k_t$, with k and k_t the laminar and turbulent thermal conductivity respectively) and $E = h + \frac{v^2}{2}$ where h is the enthalpy. The turbulent thermal conductivity is obtained with the constant turbulent Prandtl number hypothesis. The energy term for species diffusion was calculated through a user-defined function and added to the energy equation as a source term. The expression for the diffusion flux of species i, $\vec{J}_i$ is the same as for the species conservation equation (Eq. 6). h_i is the enthalpy of gas i, defined as the sum of the enthalpies of the species making up the respective gas. For model 2 and 3, h_i was defined from the directly calculated enthalpy h of the binary and ternary mixture, respectively, so that: $h(Y_i, \ldots, Y_{n-1}, T) = \sum_i^n h_i(Y_i, \ldots, Y_{n-1}, T) Y_i$ with $\sum_i^n Y_i = 1$ and with $n = 2$ (Ar and H_2O) for model 2 and $n = 3$ (Ar, H_2O and N_2) for model 3. The contribution of the enthalpies of the combined ions and molecules from the interactions between H_2O and N_2 in model 3 were included in the enthalpy of N_2. Their contribution to the enthalpy value, however, is very small because of the low concentration of these species. The last term on the right-hand side of Eq. 7 is the net radiation power R and represents the energy loss from the hot arc core by radiation. R was modeled with the net emission coefficient (NEC) approach by $R = 4\pi\varepsilon_N$ where ε_N is the net emission coefficient (W m^{-3} $s.r^{-1}$). Approximate values for the net emission coefficients for an argon/water plasma mixture with 30 % argon molar content at a pressure of 1 atm and for a plasma radius of 1.8 mm were used, taken from Aubrecht et al. [40].

Results

The flow variables selected for comparing the three mixing models are temperature, velocity and nitrogen mole fraction. Radial profiles of these variables were evaluated at different positions downstream of the torch exit nozzle (5, 20, 40, 50, 60, 90 and 150 mm). The sampled data at these positions were statistically averaged in time (over 130,000 time steps or 19.5 ms) and in space (over 8 radii at the particular cross section). For comparison of the three mixing models, the profiles are shown over a length of 1 cm radial on the jet centerline. The negative radius values were used to plot results of a chosen model against the output of a second model, plotted on the positive radius values.

In Fig. 4, the radial temperature profiles of model 1 versus model 2 are plotted. The temperature values at every position are almost identical with only small differences at the positions 40, 50 and 60 mm where the temperatures from model 2 are smaller than those from model 1. Overall, there are no big differences in the temperature field between model 1 and model 2. A different trend can be seen in Fig. 5, where for model 2 and model 3 only the temperatures in the high-temperature region of the plasma jet (dotted lines for 5 and 20 mm) are in good agreement. From 40 mm downwards, the radial temperature profiles of model 3 clearly show much higher temperatures than the profiles from model 2. The differences in centerline temperatures between model 2 and model 3 can be up to 55 % of the values calculated in model 2.

The comparison of axial velocity profiles from simulations with model 1 and model 2 is plotted in Fig. 6. Similar to the comparison of the temperature field of these two models (Fig. 4), there are some small differences in the velocity fields noticeable between 40 and 60 mm downstream of the torch exit. The velocities at these positions are slightly lower for model 2 compared to model 1. In Fig. 7, it can be seen that the velocity profiles from the simulation with model 3 show significantly higher values than the velocity profiles from the simulation with model 2 starting at 40 mm downstream of the exit nozzle. These differences increase further downstream and calculated velocities of the jet with model 3

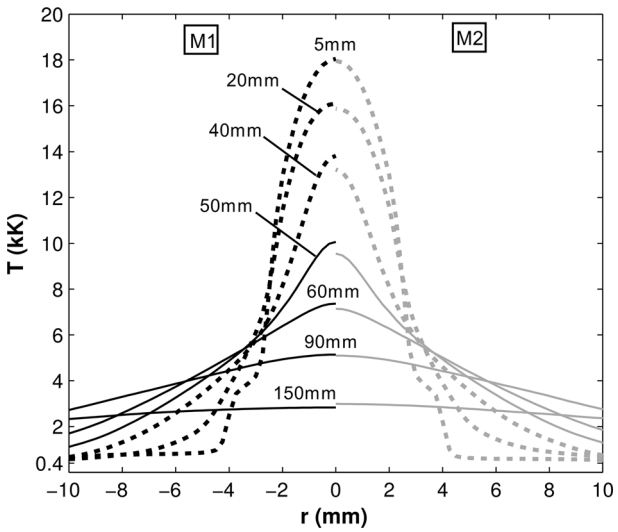

Fig. 4 Temperature profiles of model 1 (*black*) versus model 2 (*grey*)

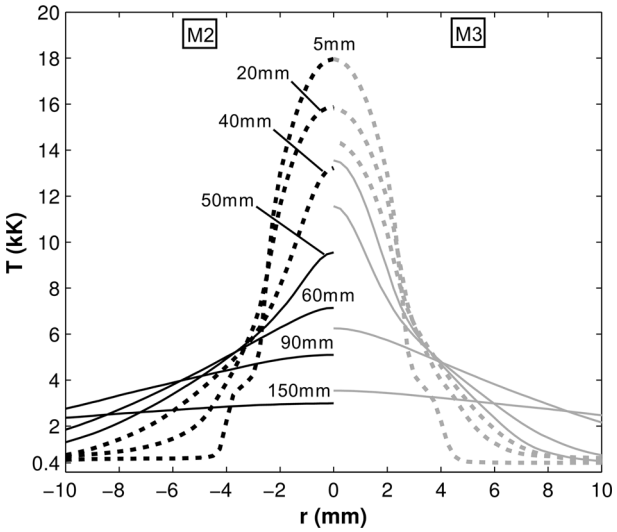

Fig. 5 Temperature profiles of model 2 (*black*) versus model 3 (*grey*)

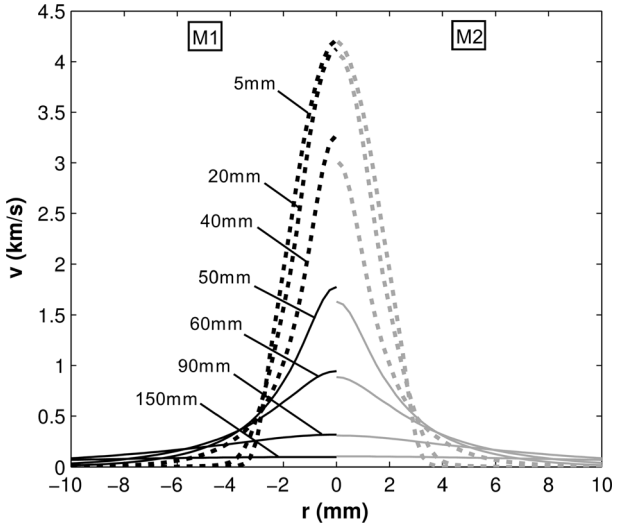

Fig. 6 Velocity profiles of model 1 (*black*) versus model 2 (*grey*)

can become more than twice as high as the ones with model 2 at the same positions (50, 60 and 90 mm).

Finally, nitrogen mole fraction is the last variable evaluated to make the comparison between the three mixing models. This parameter characterizes the level of entrainment of surrounding gas into the plasma jet. The profiles of nitrogen mole fraction of model 1 and model 2 are plotted in Fig. 8. The concentration profiles of nitrogen gas in the gas mixture are almost identical for both models. The comparison between model 2 and model 3 on the

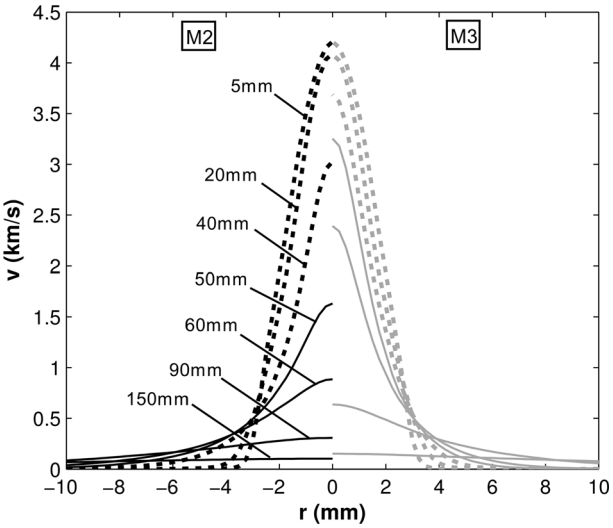

Fig. 7 Velocity profiles of model 2 (*black*) versus model 3 (*grey*)

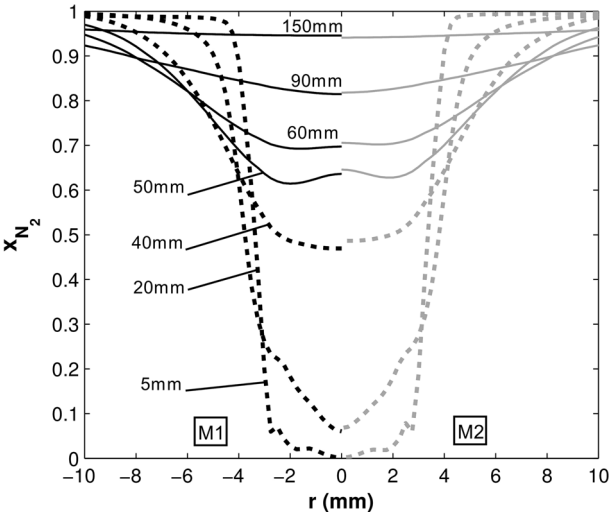

Fig. 8 Nitrogen mole fraction profiles of model 1 (*black*) versus model 2 (*grey*)

basis of nitrogen mole fraction in Fig. 9 shows different results than those in Fig. 8. In the high-temperature region (5 and 20 mm), the concentrations of nitrogen gas in the gas mixture are nearly identical for the two models, but at 40 mm and further downstream of the torch exit the profiles of nitrogen mole fraction from the simulation with model 2 are much higher than those from the simulation with model 3. As shown by the rapid increase in nitrogen concentration in the downstream direction in model 2, it is clear that the entrainment of the surrounding atmosphere occurred much faster (i.e. closer to the torch exit) with model 2 than with model 3.

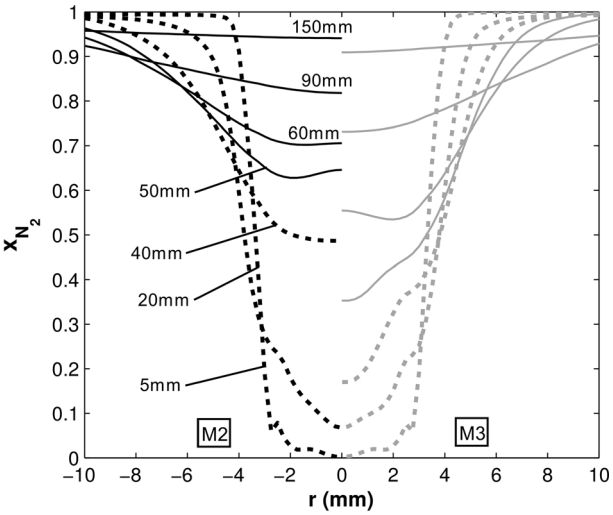

Fig. 9 Nitrogen mole fraction profiles of model 2 (*black*) versus model 3 (*grey*)

Discussion

The comparison of model 1 with model 2 in Figs. 4, 6 and 8 showed little difference in the temperature, velocity and nitrogen mole fraction profiles. This means that the correct calculation of the thermodynamic and transport properties of the plasma gas (Ar/H_2O) has only a limited influence on the flow characteristics. The full multi-component approach (model 3), on the other hand, gave a significantly different flow field than model 2 (see Figs. 5, 7, 9). Up to 20 mm from the torch exit, the profiles of temperature, velocity and nitrogen concentration are quasi-identical with model 2 and model 3. The big differences start from 20 mm downwards, where a steep increase of nitrogen mole fraction at 40 mm for model 2 can be seen. This is caused by an intense entrainment of nitrogen into the jet, which indicates turbulent mixing of the jet with the surrounding atmosphere. This is accompanied by the sharp decrease of velocity and temperature (i.e. cooling with cold nitrogen) in the simulation with model 2 from 20 mm downwards. For model 3, the increase in nitrogen mole fraction in the jet occurs more gradually, suggesting a longer, more stable jet with a delayed onset of turbulence. The observation that the jet calculated with model 3 remains quasi-laminar for a longer time than the jet calculated with model 2 is confirmed by looking at the evolution of the root-mean-square (RMS) of the velocity fluctuations at different axial positions (Fig. 10). This parameter is an indicator of the velocity fluctuations and stability of the jet, or level of turbulence. The values of this variable are much higher at positions closer to the torch exit for model 2 than for model 3. Including all interactions of the ternary gas mixture in the calculation of thermodynamic and transport properties clearly has a large impact on the flow variables.

The thermodynamic and transport properties of the gas mixture with composition 25 wt% argon, 25 wt% steam and 50 wt% nitrogen are plotted to examine which differences between the calculated values by the three models cause the differences in the resulting flow fields.

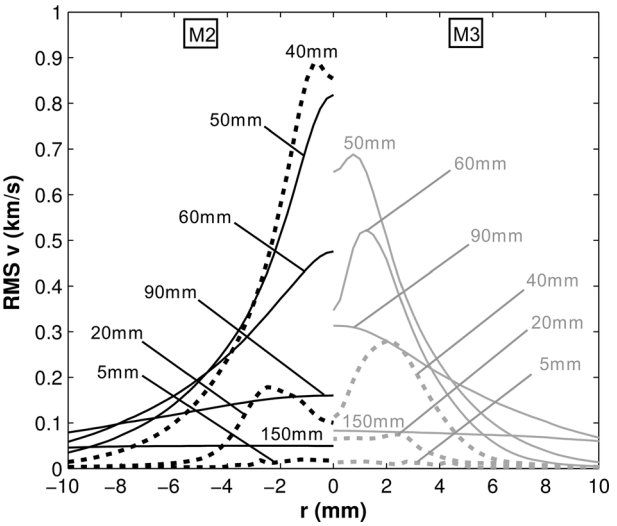

Fig. 10 Root-mean-square velocity profiles of model 2 (*black*) versus model 3 (*grey*)

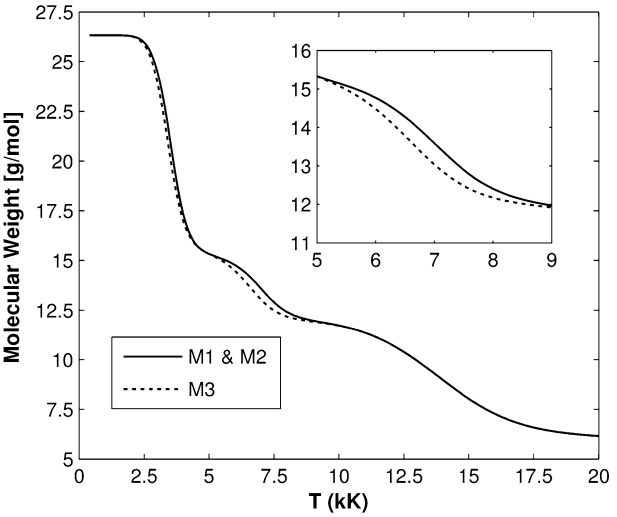

Fig. 11 Difference in molecular weight between model 1 and 2 (*full line*) and model 3 (*dotted line*) for a mixture of 25 wt% Ar, 25 wt% H_2O and 50 wt% N_2

Values of molecular weight and enthalpy of the selected mixture composition as a function of temperature are displayed in Figs. 11 and 12 respectively. Density values are not reported because no significant differences were identified between the models. In these figures, the lines for model 1 and model 2 overlap (full lines), because no errors were introduced by using mixing rules for the calculation of thermodynamic properties of the plasma gas mixture. The properties calculated by model 3 are represented by the dotted lines.

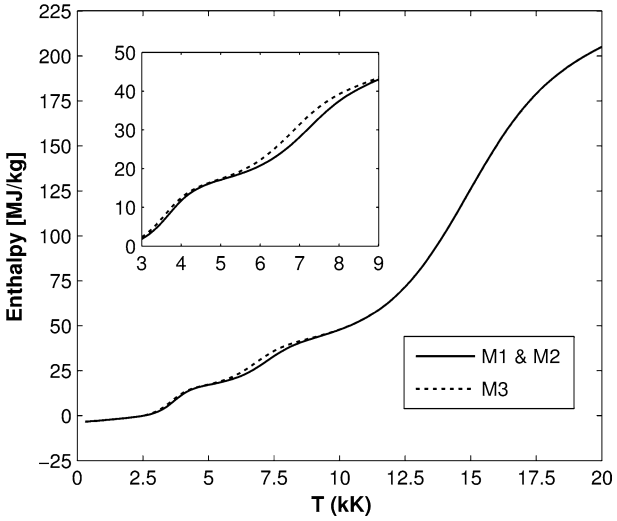

Fig. 12 Difference in enthalpy between model 1 and 2 (*full line*) and model 3 (*dotted line*) for a mixture of 25 wt% Ar, 25 wt% H_2O and 50 wt% N_2

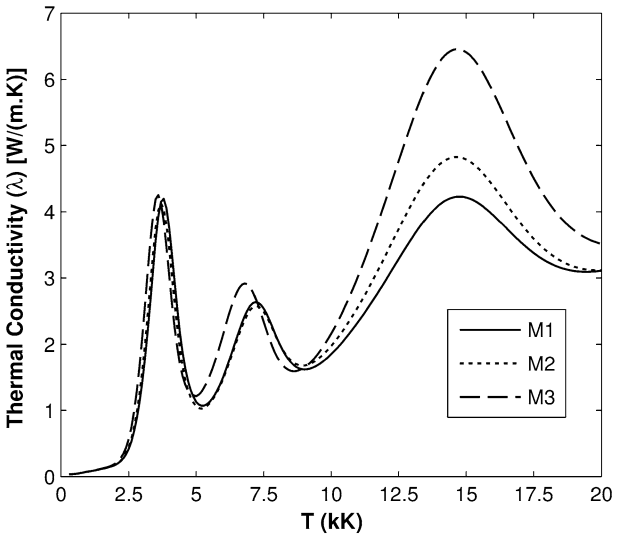

Fig. 13 Difference in thermal conductivity between model 1 (*full line*), model 2 (*short dotted line*) and model 3 (*long dotted line*) for a mixture of 25 wt% Ar, 25 wt% H_2O and 50 wt% N_2

The molecular weights and enthalpies calculated with model 3 are respectively lower and higher than the ones from model 1 and 2 between 5,000 and 9,000 K. In model 3, the products from combination of elements of water vapour and nitrogen are taken into account in the mixture composition. In this temperature range, nitric oxide (NO) and other combination species in smaller concentrations are formed and cause the differences in molecular weight and enthalpy values. However, they do not explain the large changes in the flow field

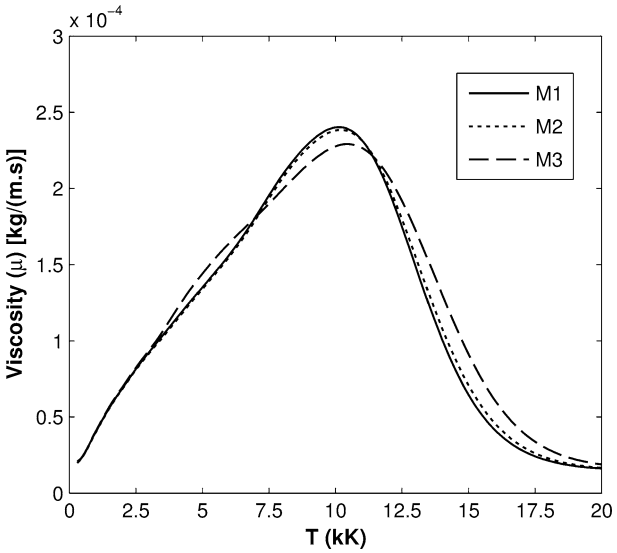

Fig. 14 Difference in viscosity between model 1 (*full line*), model 2 (*short dotted line*) and model 3 (*long dotted line*) for a mixture of 25 wt% Ar, 25 wt% H_2O and 50 wt% N_2

calculated with model 3 compared to that calculated with model 2. The reason for this can be found in the differences in transport properties between the three mixing models.

The thermal conductivity and viscosity for the same mixture composition as a function of temperature of the three models are compared respectively in Figs. 13 and 14. The full multi-component approach for the calculation of the transport properties (model 3) clearly generated different values than the other two models, which used the mixing rules of Wilke [27] and Mason and Saxena [28] for the respective properties. As noted above, these formulas were proposed for mixtures of non-ionized gases, considering only elastic collisions and employing several approximations. This does not give satisfactory results for thermal conductivity where the contribution of the inelastic collisions is important because they are responsible for the dissociation and ionization peaks apparent in Fig. 13. Consequently, the use of the mixing rule of Mason and Saxena leads to an underestimation of the actual values of thermal conductivity, especially at the ionization temperatures (between 10,000 and 20,000 K). It is clear that the differences in thermal conductivities between model 2 and model 3 are much higher than those between model 1 and model 2. In the calculation of thermal conductivity in model 2, the only additional interactions taken into account by rigorous calculation, relative to the calculation in model 1, are those between species derived from argon and water vapour. Interactions between all species in the ternary mixture are considered in the full multi-component approach of model 3, leading to much larger differences.

The higher thermal conductivities of model 2 in the high-temperature region, compared to model 1, lead to lower temperature profiles in the center of the jet (Fig. 4) because of a higher radial heat transfer. These lower temperatures in model 2 in turn lead to higher viscosities in the center of the jet and therefor lower velocities (Fig. 6).

In the explanation for the differences in flow fields between model 2 and model 3, the processes at the fringes of the jet are more important, since it is the delayed onset of

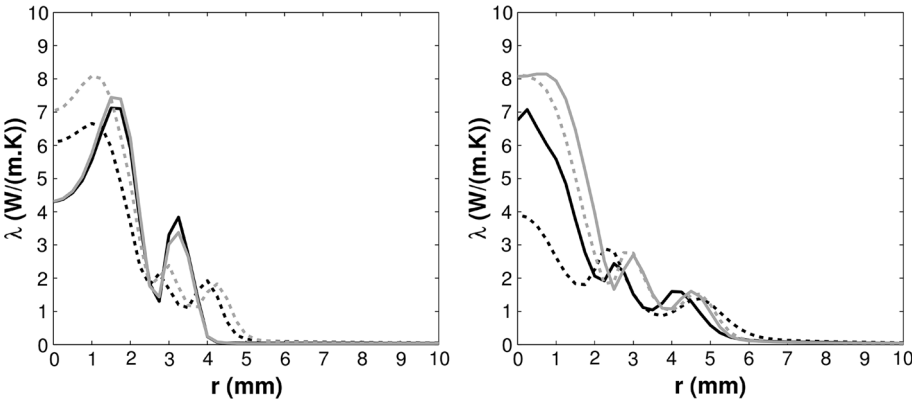

Fig. 15 Average thermal conductivity profiles of model 2 (*black*) versus model 3 (*grey*); *left-hand side*: positions 5 mm (*full line*) and 20 mm (*dashed line*) downstream of the exit nozzle; *right-hand side*: positions 30 mm (*full line*) and 40 mm (*dashed line*) downstream of the exit nozzle

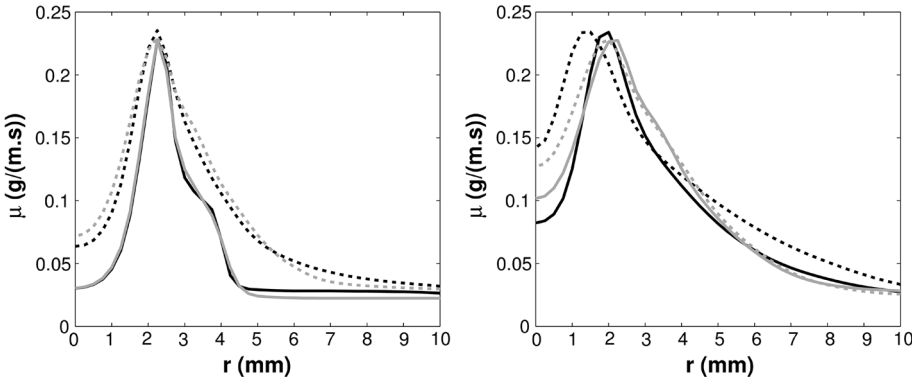

Fig. 16 Average viscosity profiles of model 2 (*black*) versus model 3 (*grey*); *left-hand side*: positions 5 mm (*full line*) and 20 mm (*dashed line*) downstream of the exit nozzle; *right-hand side*: positions 30 mm (*full line*) and 40 mm (*dashed line*) downstream of the exit nozzle

turbulence in model 3 that leads to the large differences observed. The influence of each of the thermodynamic and transport properties on this delayed onset was assessed by exchanging one-by-one, each property used in model 2 for the rigorously-calculated property used in model 3. It was found that only by changing the thermal conductivity were large differences in the flow fields obtained; changing all the other properties led to only small differences. It is therefore concluded that the different thermal conductivity values used in model 3 are primarily responsible for the delayed onset of turbulence, and the consequent changes in jet properties.

In the region close to the torch exit, the temperatures at the core of the jet range from 10,000 to 20,000 K (Fig. 5). It is clear from Fig. 13 that the values of thermal conductivity in this temperature range are strongly underestimated by the mixing law of Mason and Saxena with model 2. The higher average thermal conductivities obtained with model 3 (Fig. 15) cause higher radial heat transfer and higher temperatures at the edge of the jet

compared to model 2. Higher temperatures in the temperature range at the jet boundary (<10,000 K) lead to higher viscosities (Fig. 14). The average viscosities in the region close to the exit nozzle (Fig. 16) indeed show higher values of viscosity for model 3 than for model 2, leading to a lower Reynolds number. This limits the entrainment of nitrogen gas in the plasma jet, which is predominantly due to turbulent mixing, and results in a more stable jet (i.e. a longer transition to turbulence). This delays the cooling of the jet with cold nitrogen gas and slows down the decrease in velocity of the plasma jet.

Conclusion

In this paper, the influence of the use of mixing rules in assigning thermodynamic and transport properties to a high-temperature gas mixture in plasma jet modeling was investigated. CFD simulations of an argon/water plasma jet issuing into ambient nitrogen gas with three different mixing models were compared on the basis of the temperature, velocity and nitrogen concentration profiles in the resulting flow field.

It was found that the use of approximate mixing rules can greatly influence the calculated flow of a plasma jet. As already mentioned by Gleizes et al. [9], the specific differences in flow fields between a simulation with rigorous calculation of thermodynamic and transport properties of a gas mixture and simulations with estimation of the mixture properties by mixing rules are particular to the individual case that is modeled. However, it can be concluded that the cause of the differences are the deviations from exact values of transport properties, calculated in this case with the mixing rules of Wilke and of Mason and Saxena. The more important the interactions between the different gases (e.g. inelastic collisions between water vapour and nitrogen), the larger the error in the calculation of the transport properties, especially thermal conductivity).

In the literature, the possible effect of the errors introduced on the flow field from inaccurate values for viscosity and thermal conductivity (calculated with mixing rules) are frequently ignored by assuming that their contribution is negligible in relation to their turbulent counterparts. However, in plasma jet modeling, the level of turbulence in the high-temperature region close to the torch exit is often low and the jet can be considered as quasi-laminar. In that region, the values of the molecular transport properties are much higher than those of the turbulent transport properties. Our results demonstrate that these effects can strongly influence the onset of turbulence, and consequently the properties of the flow in the turbulent regions, calculated from CFD simulations. Exact calculation of the transport properties is therefore necessary for a correctly calculated plasma flow.

Acknowledgments The author gratefully acknowledges the support of this work by the Agency for Innovation by Science and Technology in Flanders (IWT).

Appendix 1: Expression for the Diffusion Flux in a Three-Component Mixture in Terms of Binary Combined Diffusion Coefficients

A gas mixture of Ar (A), H_2O (B) and N_2 (C) is considered. The diffusion flux of gas A (consisting of species 1 to p) can be written as:

$$\bar{J}_A = \frac{n^2}{\rho} \sum_{i=1}^{p} k_i m_i \sum_{j=1}^{q} m_j D_{ij} \nabla x_j^{(3)} - \sum_{i=1}^{p} k_i D_i^T \nabla \ln T \tag{8}$$

in which $i = 1,\ldots,q$ corresponds to the species making up gas B and C. $x_j^{(3)}$ represents the mole fraction of species j in the three-component gas mixture. For further details on the derivation of this expression, see Murphy [38].

Because the mole fraction of species j ($x_j^{(3)}$) is function of temperature and composition, and because composition is determined by the mole fractions of two out of three gases, the gradient of the mole fraction becomes:

$$\nabla x_j^{(3)} = \left.\frac{\partial x_j^{(3)}}{\partial x_B}\right|_{x_C,T} \nabla x_B + \left.\frac{\partial x_j^{(3)}}{\partial x_C}\right|_{x_B,T} \nabla x_C + \left.\frac{\partial x_j^{(3)}}{\partial T}\right|_{x_B,x_C} \nabla T \tag{9}$$

in which x_B and x_C are respectively the mole fractions of gas B and gas C at temperature T. The species 1 to q are the collection of species originating from both gas B and gas C. Since no combination species are considered between species from B and species from C, the species $1,\ldots,q$ can be split up into $1,\ldots,q_B$ (species from gas B) and $q_B + 1,\ldots,q_C$ (species from gas C). The following relations are then being considered:

$$\text{For } j = 1,\ldots,q_B : \left.\frac{\partial x_j^{(3)}}{\partial x_C}\right|_{x_B,T} \cong 0 \text{ and for } j = q_B + 1,\ldots,q_C : \left.\frac{\partial x_j^{(3)}}{\partial x_B}\right|_{x_C,T} \cong 0 \tag{10}$$

For $j = 1,\ldots,q_B$:

$$\left.\frac{\partial x_j^{(3)}}{\partial T}\right|_{x_B,x_C} \cong \left.\frac{\partial x_j^{(2)}}{\partial T}\right|_{x_B} \tag{11}$$

$$\left.\frac{\partial x_j^{(3)}}{\partial x_B}\right|_{x_C,T} \cong \left.\frac{\partial x_j^{(2)}}{\partial x_B}\right|_{T} \tag{12}$$

with $x_j^{(2)}$ the mole fraction of species j in the binary gas mixture of A and B with the same mole fraction of gas B, x_B as in the three-component gas mixture.For $j = q_B + 1,\ldots,q_C$:

$$\left.\frac{\partial x_j^{(3)}}{\partial T}\right|_{x_B,x_C} \cong \left.\frac{\partial x_j^{(2)}}{\partial T}\right|_{x_C} \tag{13}$$

$$\left.\frac{\partial x_j^{(3)}}{\partial x_C}\right|_{x_B,T} \cong \left.\frac{\partial x_j^{(2)}}{\partial x_C}\right|_{T} \tag{14}$$

with $x_j^{(2)}$ the mole fraction of species j in the binary gas mixture of A and C with the same mole fraction of gas C, x_C as in the three-component gas mixture.

With the definitions of combined diffusion coefficients:

$$\bar{D}_{AB}^{x} = \frac{1}{m_A m_B} \sum_{i=1}^{p} k_i m_i \sum_{j=1}^{q_B} m_j D_{ij} \left.\frac{\partial x_j^{(2)}}{\partial \bar{x}_B}\right|_{T} \tag{15}$$

$$\bar{D}_{AC}^{x} = \frac{1}{m_A m_C} \sum_{i=1}^{p} k_i m_i \sum_{j=q_B+1}^{q_C} m_j D_{ij} \left.\frac{\partial x_j^{(2)}}{\partial \bar{x}_C}\right|_{T} \tag{16}$$

$$\bar{D}_{AB}^{T} = -\frac{n^2}{\rho}\sum_{i=1}^{p} k_i m_i \sum_{j=1}^{q_B} m_j D_{ij} \left.\frac{\partial x_j^{(2)}}{\partial T}\right|_{x_B} + \sum_{i=1}^{p} k_i D_i^{T(AB)} \tag{17}$$

with $D_i^{T(AB)}$ the thermal diffusion coefficient of species i in the binary mixture of A and B

$$\bar{D}_{AC}^{T} = -\frac{n^2}{\rho}\sum_{i=1}^{p} k_i m_i \sum_{j=q_B+1}^{q_C} m_j D_{ij} \left.\frac{\partial x_j^{(2)}}{\partial T}\right|_{x_C} + \sum_{i=1}^{p} k_i D_i^{T(AC)} \tag{18}$$

with $D_i^{T(AC)}$ the thermal diffusion coefficient of species i in the binary mixture of A and C

The diffusion flux of gas A becomes:

$$\begin{aligned}\bar{J}_A = {} & \frac{n^2}{\rho}\left(m_A m_B \bar{D}_{AB}^{x}(x_B, T)\nabla x_B + m_A m_C \bar{D}_{AC}^{x}(x_C, T)\nabla x_C\right) \\ & - \bar{D}_{AB}^{T}(x_B, T)\nabla \ln T - \bar{D}_{AC}^{T}(x_C, T)\nabla \ln T + S\end{aligned} \tag{19}$$

with the extra term S:

$$S = \sum_{i=1}^{p} k_i D_i^{T(AB)} \nabla \ln T + \sum_{i=1}^{p} k_i D_i^{T(AC)} \nabla \ln T - \sum_{i}^{p} k_i D_i^{T(3)} \nabla \ln T \tag{20}$$

in which $D_i^{T(3)}$ is the thermal diffusion coefficient of species i in the three-component mixture. The term S consists of the terms describing the Soret effect, which is considered small, therefore the term S is neglected in the expression for the diffusion flux of gas A in the three-component mixture of A, B and C.

References

1. Boussagol A, Mariaux G, Legros E, Vardelle A, Nylen P (2001) 3-D modeling of a DC plasma jet using different commercial CFD codes. In: Proceedings of 15th international symposium on plasma chemistry, Orléans, France, GREMI CNRS, pp 1015–1020
2. Mariaux G, Vardelle A (2005) 3D time-dependent modeling of the plasma spray process, part 1: flow modeling. Int J Therm Sci 44:357–366
3. Murphy AB (1996) A comparison of treatments of diffusion in thermal plasmas. J Phys D Appl Phys 29:1922–1932
4. Balmigere G, Meillot E, Vincent S, Caltagirone J-P (2007) Unsteady 3D large eddy simulation of an Ar–H_2 plasma jet: analysis of initial results. In: Thermal spray: global coating solutions, pp 185–189
5. Cheng K, Chen X, Pan W (2006) Comparison of laminar and turbulent thermal plasma jet characteristics—a modeling study. Plasma Chem Plasma Process 26:211–235
6. Selvan B, Ramachandran K (2009) Comparisons between two different three-dimensional arc plasma torch simulations. J Therm Spray Technol 18(5–6):846–857
7. Trelles JP, Chazelas C, Vardelle A, Heberlein JVR (2009) Arc Plasma torch modeling. J Therm Spray Technol 18(5–6):728–752
8. Murphy AB, Arundell CJ (1994) Transport coefficients of argon, nitrogen, oxygen, argon–nitrogen and argon–oxygen plasmas. Plasma Chem Plasma Process 14:451–490
9. Gleizes A, Cressault Y, Teulet Ph (2010) Mixing rules for thermal plasma properties in mixtures of argon, air and metallic vapours. Plasma Sources Sci Technol 19:1–13
10. Coufal O, Sezemsky P, Živný O (2005) Database system of thermodynamic properties of individual substances at high temperatures. J Phys D Appl Phys 38:1265–1274
11. Coufal O (2007) Composition and thermodynamic properties of thermal plasma up to 50kK. J Phys D Appl Phys 40:3371–3385
12. Krenek P (2008) Thermophysical properties of H_2O–Ar plasmas at Temperatures 400–50,000 K and pressure 0.1 MPa. Plasma Chem Plasma Process 28:107–122
13. Li H-P, Chen X (2001) Three-dimensional modeling of a DC non-transferred arc plasma torch. J Phys D Appl Phys 34:L99–L102

14. Li H-P, Pfender E (2007) Three dimensional modeling of the plasma spray process. J Therm Spray Technol 16(2):245–260
15. Huang R, Fukanuma H, Uesugi Y, Tanaka Y (2011) An improved local thermal equilibrium model of DC arc plasma torch. IEEE Trans Plasma Sci 39(10):1974–1982
16. Dilawari AH, Szekely J, Westhoff R, Detering BA, Shaw CB Jr., (1991) A comparison of the experimentally measured and theoretically predicted temperature profiles for an argon jet discharging into a nitrogen environment. Mater Res Soc Proc 190:199–205
17. Westhoff R, Szekely J (1991) A model of fluid, heat flow, and electromagnetic phenomena in a nontransferred arc plasma torch. J Appl Phys 70(7):3455–3466
18. Guenadou D, Meillot E, Saget A (2005) Particle treatment modeling in a time-dependent DC plasma flow. In: Thermal spray connects: explore its surfacing potential! pp 326–331
19. Eichert P, Imbert M, Coddet C (1998) Numerical study of an Ar–H_2 gas mixture flowing inside and outside a DC plasma torch. J Therm Spray Technol 7(4):505–512
20. Meillot E, Vincent S, Caruyer C, Caltagirone J-P, Damiani D (2009) From DC time-dependent thermal plasma generation to suspension plasma-spraying interactions. J Therm Spray Technol 18(5–6):875–886
21. Meillot E, Guenadou D, Bourgois C (2008) Three-dimension and transient DC plasma flow modeling. Plasma Chem Plasma Process 28:69–84
22. Baudry C, Mariaux G, Vardelle A, Delalondre C, Meillot E (2003) Modeling of arc formation in a DC plasma spray torch. In: Proceedings of ISPC-16, Taormina, Italy, Wiley
23. Vincent S, Balmigere G, Caruyer C, Meillot E, Caltagirone J-P (2009) Contribution to the modeling of the interaction between a plasma flow and a liquid jet. Surf Coat Technol 203:2162–2171
24. Gleizes A, Gonzalez JJ, Freton P (2005) Thermal plasma modelling. J Phys D Appl Phys 38:R153–R183
25. Trelles JP, Pfender E, Heberlein J (2006) Multiscale finite element modeling of arc dynamics in a DC plasma torch. Plasma Chem Plasma Process 26:557–575
26. Colombo V, Ghedini E, Sanibondi P (2010) A three-dimensional investigation of the effects of excitation frequency and sheath gas mixing in an atmospheric-pressure inductively coupled plasma system. J Phys D Appl Phys 43(1):13
27. Wilke CR (1950) A viscosity equation for a gas mixture. J Chem Phys 18(4):517–519
28. Mason EA, Saxena SC (1958) Approximate formula for the thermal conductivity of gas mixture. Phys Fluids 1(5):361–369
29. Murphy AB (2012) Transport coefficients of plasmas in mixtures of nitrogen and hydrogen. Chem Phys 398:64–72
30. Palmer GE, Wright MJ (2003) Comparison of methods to compute high-temperature gas viscosity. J Thermophys Heat Transf 17(2):232–239
31. Hrabovský M, Kopecký V, Sember V, Kavka T, Chumak O, Konrád M (2006) Properties of hybrid water/gas DC arc plasma torch. IEEE Trans Plasma Sci 34(4):1566–1575
32. Williamson RL, Fincke JR, Crawford DM, Snyder SC, Swank WD, Haggard DC (2003) Entrainment in high-velocity, high-temperature plasma jets. Part II: computational results and comparison to experiment. Int J Heat Mass Transf 46:4215–4228
33. Lorcet H, Brothier M, Guenadou D, Latge C, Vardelle A (2010) Modeling bio-oil gasification by a plasma process. High Temp Mater Process 14:11–27
34. Hrabovský M, Konrád M, Kopecký V, Sember V (2003) In: Solonenko OP (ed) Thermal plasma torches and technologies, 1st edn. Cambridge International Science Publishing, Cambridge
35. Murphy AB, Tam E (2014) Thermodynamic properties and transport coefficients of arc lamp plasmas: argon, krypton and xenon. J Phys D Appl Phys 47: 295202 (10p)
36. Murphy AB (2000) Transport coefficients of hydrogen and argon–hydrogen plasmas. Plasma Chem Plasma Process 20:279–297
37. Murphy AB (1995) Transport coefficients of air, argon–air, nitrogen–air, and oxygen–air plasmas. Plasma Chem Plasma Process 15:279–307
38. Boulos M, Fauchais P, Pfender E (1995) Thermal plasmas: fundamental and applications. Plenum Press, New York
39. Murphy AB (1993) Diffusion in equilibrium mixtures of ionized gases. Phys Rev E 48:3594–3603
40. Aubrecht V, Bartlova M, Urban F, Valenta J (2004) Partial characteristics of radiation for thermal plasmas in H_2O and argon. In: Proceedings of 15th international conference on gas discharges and their applications, Toulouse, France, pp 141–144